Afr Archaeol Rev (2024) 41:97–118
https://doi.org/10.1007/s10437-023-09552-7

ORIGINAL ARTICLE

Production and Use of Ceramics in the First Millennium BC: Jebel Moya, Sudan

Mantas Valancius · Patrick Quinn · Michael Brass · I. Vella Gregory · Ahmed Adam · Julie Dunne · Richard P. Evershed

Accepted: 10 August 2023 / Published online: 16 September 2023

Abstract The site of Jebel Moya, situated in the center of the southern Gezira Plain in southcentral Sudan, has an occupational sequence spanning at least five millennia until around 2000 years ago. Renewed excavation is shedding new light on its occupational chronology and socioeconomic history, including activities such as burial, savanna herding, and domesticated sorghum cultivation practices dating to at least the mid-third millennium BC. In the present study, predominantly final phase pottery sherds from the first millennium BC to the start of the first millennium AD (Assemblage 3) have been analyzed via a combination of thin section petrography and instrumental geochemistry to determine their raw materials and place of manufacture and reconstruct their manufacturing technology. Organic residue analysis was also conducted to identify the products processed within vessels found at the site. The results suggest the existence of a well-developed local ceramic craft tradition that persisted for over one thousand years. Pots from Assemblage 3 were used to process, store, and consume animal and plant products, thus reinforcing emerging evidence for early agro-pastoral activities.

Résumé Le site de Jebel Moya, situé au centre de la plaine méridionale de Gezira dans le centre-sud du Soudan, a une séquence d'occupation s'étendant sur au moins cinq millénaires jusqu'à il y a environ 2000 ans. Des fouilles renouvelées jettent un nouvel éclairage sur sa chronologie professionnelle et son histoire socio-économique, y compris des activités telles que l'inhumation, l'élevage de savane et les pratiques de culture du sorgho domestiqué datant d'au moins le milieu du troisième millénaire avant notre ère. Dans la présente étude, principalement des tessons de poterie de la phase finale du premier millénaire avant J. reconstruire leur technologie de fabrication. Une analyse des résidus organiques a également été effectuée pour identifier les produits transformés dans les cuves trouvées sur le site. Les résultats suggèrent l'existence d'une tradition artisanale céramique locale bien développée qui a persisté pendant plus de mille ans. Les pots de l'assemblage 3 ont été utilisés pour transformer, stocker et consommer des produits animaux et

M. Valancius
Lithuanian Institute of History, Tilto G. 17, 01101 Vilnius, Lithuania

P. Quinn · M. Brass (✉)
Institute of Archaeology, University College London, 31-34 Gordon Square, London WC1H 0PY, UK
e-mail: michael.brass@ucl.ac.uk

I. Vella Gregory
MacDonald Institute for Archaeological Research, Downing Street, Cambridge CB2 3ER, UK

A. Adam
Department of Archaeology, University of Khartoum, Al-Nil Avenue, Khartoum, Sudan

J. Dunne · R. P. Evershed
Organic Geochemistry Unit, School of Chemistry, University of Bristol, Cantock's Close, Bristol BS8 1TS, UK

végétaux, renforçant ainsi les preuves émergentes des premières activités agro-pastorales.

Keywords Sudan · Jebel Moya · Pottery · Petrography · Lipid residue · Agro-pastoralism

Introduction

Jebel Moya is a granite massif that rises from the Gezira Plain in Central Sudan, south of the capital Khartoum and halfway between Sennar on the Blue Nile and Rabak on the White Nile (Fig. 1a). In the northeast corner of the range is a valley 10.4 hectares in size whose official designation is Site 100 but is more commonly referred to by the name of the massif. It was first excavated by Henry Wellcome (1911–1914) and more recently by The University College London–University of Khartoum-National Museum of Antiquities and Museums (UCL–UoK-NCAM) Expedition to the Southern Gezira (Brass, 2016; Brass & Vella Gregory, 2021; Brass et al., 2019, 2020; Vella Gregory, 2020). It is one of the few sites currently being excavated south of Khartoum.

The site has so far yielded 3141 human burials, most excavated by Henry Wellcome's team (Addison, 1949). The present expedition is shedding light on the previously unknown history of southern Gezira. The earliest known habitation layers in this large site are currently attributed to the late sixth millennium BC (Brass & Vella Gregory, 2021; Brass et al., 2018). However, the ongoing excavations have yet to reach sterile layers or bedrock. Domesticated cattle, sheep or goats, and early domesticated sorghum were present at Jebel Moya by the early-mid third millennium BC. The earliest known human burial is AMS-dated to C. 2350 BC (Brass et al., 2019). Located outside the southernmost boundary of the Napatan and Meroitic states (Brass, 2015), the final phase of occupation is currently placed between the first millennium BC and the early first millennium AD (Vella Gregory et al., 2022) .

Due to the lack of visual microstratigraphy, excavating in small 10 cm spits within the microgeological strata provided a good measure of control (Brass et al., 2020). Three macro-level phases of occupation are discernible so far from radiocarbon dates (Brass et al., 2019; Brass & Vella Gregory, 2021; Vella Gregory et al., 2022), and these can be correlated with the macro-geological strata termed A–D:

- Phase 1. This late sixth millennium BC phase encompasses Stratum D and pottery Assemblage 1.
- Phase 2. It begins in the third millennium BC and continues into the second millennium BC. It is represented by pottery Assemblage 2 and is predominantly in Stratum C. Burial activity occurred in this phase.
- Phase 3. This first millennium BC to early first millennium AD phase encompasses strata A and B and pottery Assemblage 3. Considerable burial activity occurred in this phase.

Pottery forms a significant part of the material culture at Jebel Moya and contains key evidence for potential connections between the site and the surrounding areas (Brass & Vella Gregory, 2021). It also has the potential to inform the subsistence strategies and the nature of mobility of the local agro-pastoral community (Gosselain, 2000, 2010; Gosselain & Livingstone Smith, 2013). The excavated pottery has been subdivided into three distinct assemblages based on single and co-occurring attributes (Brass & Vella Gregory, 2021). These attributes are the variety and types of tools used, their motor actions, and the resulting décor on different rim types and sherd bodies.

In the present study, a sample of recently excavated pottery sherds predominantly originating from Assemblage 3 (first millennium BC) was analyzed in order to shed light on their raw materials, production location(s), manufacturing technology, and use(s). The study is the second of its kind south of Khartoum (Del Sasso et al., 2014) and the first for the time period, which means there are no comparative samples from southcentral Sudan. This is an area where detailed localized geological data needs to be built up.

The inorganic composition of the paste was investigated using thin-section ceramic petrography and instrumental geochemistry. At the same time, organic residue analysis was conducted using gas chromatography (GC), gas chromatography-mass spectrometry (GC–MS), and gas chromatography-combustion-isotope ratio mass spectrometry (GC-C-IRMS). The results are used to tackle several research questions: Firstly, was pottery locally produced or brought to

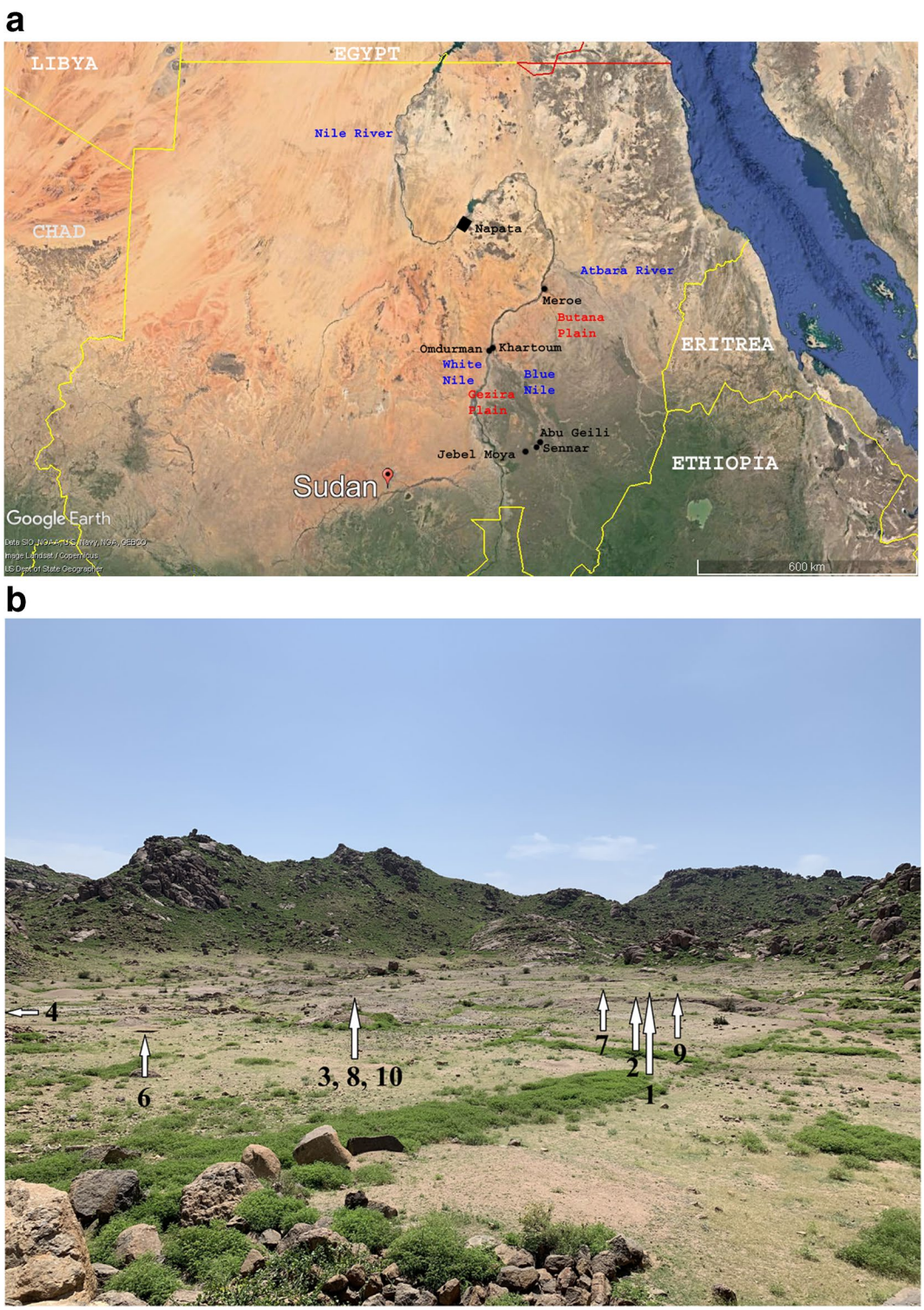

Fig. 1 **a.** Geological map of Sudan showing the location of Jebel Moya in the Gezira Plain and **b.** Jebel Moya with the locations of the ten excavated trenches from 2017 to 2019. Photograph was taken facing south from the House of the Boulders

the site from other areas? Second, can one or more pottery-making traditions be detected at the site, and how far back do they date? Third, what functions did the ceramic vessels serve at the site? By addressing these topics, the study aims to shed light on how the agro-pastoral communities of Jebel Moya and the Gezira Plain functioned outside the direct political control of the Napatan and Meroitic states.

Materials and Methods

Ceramic Compositional Analysis

A total of 62 sherds were selected from the 2017 season when the vast majority of Assemblage 3 sherds were excavated for the purpose of inorganic compositional analysis (Fig. (2; Table 1). The sherds come from in-situ habitation spits and not burial contexts; there was no sherd in unequivocal association with the one burial excavated during this season. Sherds with decorative motifs (Fig. (2) were selected to permit comparisons between the tools and motor actions used and the paste composition from which the sherds were manufactured. These sherds came from secure contexts from Trenches 1, 2, and 4 (Fig. 1b) and three sherds from surface finds. Of the 62 sherds, three earlier sherds from Assemblages 1 and 2 were also included as outliers.

The small size of the sherds prevented accurate reconstruction of the shape and size of their parent vessels. Decorated sherds number 32 (Fig. 2), of which 29 were rim sherds and one was a handle fragment. The rim shape is predominantly thin and straight ($n=21$), with eight being everted. Fifteen rim sherds were angled at 90° or less, and three were greater than 90°. Very few signs of primary forming were visible on the sherds, perhaps because of their small size and the predominance of smoothing or burnishing on the exterior. A stylus or comb were the most commonly used tools for decoration (Fig. 2). Comb stamping ($n=10$) (Fig. 2D, E) is the dominant decoration, with stylus incised lines ($n=7$) and stylus incised chevrons ($n=5$) also frequent. One sample was decorated using a seedpod, and another had fingernail impressions. The two sherds from Assemblage 2 had a thick, everted rim with incised chevrons, a rocker comb-stamped body, and a rim with stylus incisions. The single body sherd ascribed to Assemblage 1 was decorated with rocker comb stamping.

All 62 sherds were characterized and classified compositionally using a combination of thin-section petrography and instrumental geochemistry. Thin sections were made using a modification of the standard geological technique (Humphries, 1992; Quinn, 2022, p. 23–36) and analyzed under a polarizing light microscope at magnifications of ×40, ×100, and ×200. The first step in the petrographic analysis was to visually divide the thin sections into "fabrics" based on similarities and differences in their inclusions, ceramic matrix, and texture, representing distinct "recipes" characterized by specific raw materials and paste preparation techniques. The resulting fabrics were described using the system of Quinn (2022, p. 98–124). The petrographic composition of the sherds was contextualized via published geological information (Adamson et al., 1987; Ministry of Energy & Mines, Geological & Mineral Resources, 1981; Vail, 1982) in order to determine likely raw material sources and production location or provenance of the ceramics. In addition, three sand samples collected within Trenches 1 and 2 from strata dated to Assemblage 3 were mounted in epoxy, thin-sectioned, and compared to the ceramic sherds under the petrographic microscope.

Geochemical data were recorded using an Olympus Innox-X Delta Premium portable X-ray fluorescence spectroscopy (pXRF) machine with a rhodium (Rh) source and a 2-mm aluminum filter. Each measurement was taken for 120 s of live time at 40 kV. In order to address concerns about the quality of pXRF data (e.g., Speakman & Shackley, 2013), an in-house calibration developed especially for ceramics was used (Burton et al., 2019, 2021; Lewis et al., 2020; Quinn et al., 2020; Sorresso & Quinn, 2020). The pXRF spectra were deconvoluted in Brukker ARTAX software to correct for the interferences, including Rb Kß/Y Kα, Y Kß/Nb Kα, and Sr Kß/Zr Kα. The disturbance from the varying surface shape of the pottery was accounted for with a Rayleigh scatter distance correction. The in-house calibration was developed using a series of homogeneous fired spiked clay samples with four concentrations of the elements Fe, Ga, Nb, Rb, Sr, Ti, Y, and Zr (Wilke et al., 2016). These samples represent a mass absorption of mid-Z elements in a broad range of clay and other aluminosilicates, with more than 90% of the matrix composed of

Table 1 Details of 62 pottery sherds from Jebel Moya, analyzed by thin-section petrography and instrumental geochemistry

Sample	Assemblage	Trench	Spit	Vessel part	Décor	Tool	Thickness	Rim form
JMC001	3	1	1	Rim	USCS, impressed dots	Comb	11	Simple
JMC002	3	1	1	Body	N/A	N/A	6	NA
JMC003	3	1	1	Body	USCS	Comb	5	NA
JMC004	3	1	1	Body	USCS	Comb	7	NA
JMC005	3	1	1	Body	N/A	N/A	10	NA
JMC006	3	1	1	Rim	ESCS, impressed short lines	Comb	12	Simple
JMC007	3	1	1	Body	N/A	N/A	7	NA
JMC008	3	1	1	Body	USCS, dragged lines	Comb	9	NA
JMC009	3	1	1	Body	N/A	N/A	8	NA
JMC010	3	1	1	Body	N/A	NA	10	NA
JMC011	3	1	1	Body	N/A	N/A	7	NA
JMC012	3	1	1	Body	Incised lines	Stylus	8	NA
JMC013	3	1	3	Body	N/A	N/A	11	NA
JMC014	3	1	3	Rim	Chevron	Stylus	11	NA
JMC015	3	1	3	Rim	Chevron	Stylus	11	Simple
JMC016	3	1	3	Rim	Incised lines, applique paw print	Stylus	8	Simple
JMC017	3	1	3	Body	N/A	N/A	11	NA
JMC018	3	1	3	Rim	Dragged lines	Comb	16	Simple
JMC019	3	1	3	Body	N/A	N/A	12	NA
JMC020	3	1	3	Body	N/A	N/A	12	NA
JMC021	3	1	3	Rim	Impressed dots	N/A	8	Simple
JMC022	3	1	4	Rim	USCS, impressed short lines	Comb	10	Simple
JMC023	3	1	4	Rim	USCS, impressed short lines	Comb	11	Simple
JMC024	3	1	4	Rim	USCS, impressed short lines	Comb	9	Simple
JMC025	3	1	4	Rim	USCS, impressed short lines	Comb	10	Simple
JMC026	3	1	4	Body	Incised line	Stylus	6	NA
JMC027	3	1	4	Rim	Notchings	N/A	11	Simple
JMC028	3	1	4	Body	N/A	N/A	4	NA
JMC029	3	1	4	Body	N/A	N/A	8	NA
JMC030	3	1	4	Body	N/A	N/A	5	NA
JMC031	3	1	5	Handle	USCS, incised lines	Comb, Stylus	14	NA
JMC032	3	1	5	Rim	Incised lines	Stylus	9	Simple
JMC033	3	2	8	Body	Impressed lines	N/A	8	NA
JMC034	3	2	8	Body	N/A	N/A	6	NA
JMC035	3	2	8	Body	N/A	N/A	4	NA
JMC036	3	2	8	Rim	Chevron	Stylus	15	Simple
JMC037	3	2	8	Rim	N/A	N/A	7	Inverted
JMC038	3	2	8	Rim	N/A	N/A	7	Simple
JMC039	3	2	8	Body	N/A	N/A	8	NA
JMC040	3	2	8	Rim	Fingernail impressions	N/A	10	Inverted
JMC041	3	2	8	Rim	Incised lines	Stylus	18	Simple
JMC042	3	2	8	Body	N/A	N/A	11	NA
JMC043	3	2	8	Body	N/A	N/A	8	NA
JMC044	3	2	8	Body	N/A	N/A	10	NA
JMC045	3	2	8	Rim	ESCS	Comb	11	Inverted

Table 1 (continued)

Sample	Assemblage	Trench	Spit	Vessel part	Décor	Tool	Thickness	Rim form
JMC046	3	4	3	Rim	Incised lines, fingernail impressions	Stylus	15	Inverted
JMC047	3	4	3	Rim	Incised crosshatching, fingernail impressions	Stylus	18	Inverted
JMC048	3	4	3	Rim	Incised lines, impressed dots	Stylus, Seedpod	14	Inverted
JMC049	3	4	4	Body	Incised chevron	Stylus	17	NA
JMC050	3	4	4	Rim	Notchings, incised lines	Stylus	8	NA
JMC051	3	4	4	Rim	Incised lines, impressed dots, applique knobs	Stylus	12	NA
JMC052	3	4	4	Rim	Chevron, fingernail impressions	Stylus	13	Inverted
JMC053	3	4	4	Body	N/A	N/A	7	NA
JMC054	3	4	4	Rim	N/A	N/A	8	Simple
JMC055	3	4	7	Body	N/A	N/A	15	NA
JMC056	3	4	7	Body	N/A	N/A	12	NA
JMC057	3	4	7	Rim	USCS	Comb	10	Simple
JMC058	3	4	7	Rim	N/A	N/A	6	Simple
JMC059	3	4	7	Body	N/A	N/A	7	NA
JMC060	2	Surface	Surface	Body	Applique lines with incisions	Stylus	18	NA
JMC061	1	Surface	Surface	Body	Rocker comb stamping	Comb	8	NA
JMC062	2	Surface	Surface	Rim	Chevrons, USCS rocker technique	Stylus, Comb	24	Inverted

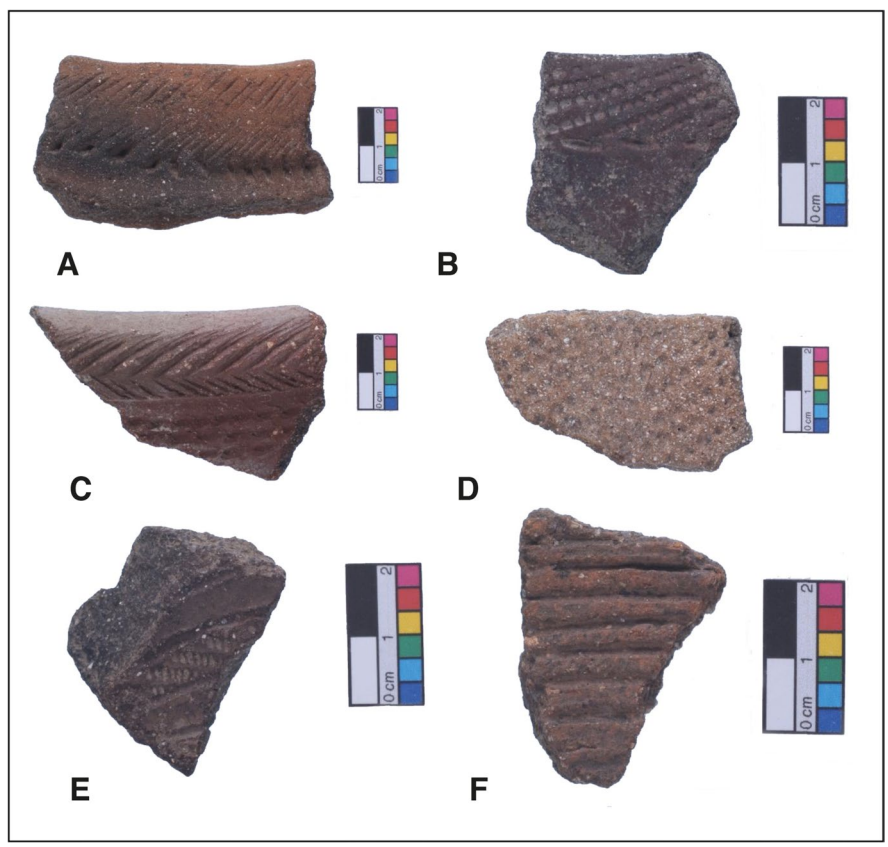

Fig. 2 Selected decorated pottery sherds from Assemblages 1, 2, and 3. **A** Stylus incised diagonal lines, sample JMC046, Assemblage 3. **B** Diagonal comb stamps, sample JMC023, Assemblage 3. **C** Rolled rim, sample JMC062, Assemblage 2. **D** Comb stamp, sample JMC061, Assemblage 1. **E** Comb stamp framed by dragged lines, sample JMC008, Assemblage 3. **F** "Grooved" pottery, sample JMC012, Assemblage 3

Al, O, and Si. In total, the calibration measured 15 elements: Ca, Co, Cu, Fe, Ga, K, Mn, Nb, Pb, Rb, Sr, Ti, Y, Zn, and Zr. In order to account for the small (*c*. 1 cm^2) beam of the pXRF and possible heterogeneity in coarse ceramics (Tykot, 2016), at least three spots were analyzed on every sherd, and their measurements were averaged after calibration. The accuracy of the instrument and the "UCL pXRF < 10% Ca calibration 2" applied to the Jebel Moya ceramics was assessed using 14 certified reference materials (CRMs) of rock, ore, sediment, soil, and ceramic (OSM 1). Each CRM was analyzed five times and calibrated using the above protocol. The averages of the five measurements were compared to the certified values for the standards that occur within the range of composition found in earthenware archaeological ceramics, as determined using the data in several published geochemical studies (Day et al., 2011; Quinn et al., 2010; Quinn & Burton, 2015; Travé Allepuz et al., 2014), and accuracy was calculated as percentage relative difference using the formula: (measured – certified/certified) × 100 (OSM 1).

The multivariate geochemical data collected on the 62 sherds were explored using principal component analysis (PCA) both in its raw state and after transformation to base 10 logarithms and the geometric mean (Baxter, 2015, p. 41). Bivariate scatter plots of the PCA scores and pairs of specific elements were used to detect similarities and differences in the bulk composition of the sherds. The resulting geochemical groupings were compared to the petrographic classification of the pottery to check for correspondence and reconcile the two in terms of the mineral and rock sources of specific elements.

Lipid Residue Analysis

Analytical Methods

Lipid residue analysis was performed on a separate set of 50 sherds randomly selected (but based on size criteria) from Assemblage 3, originating from trenches 1, 2, and 4. Lipid analysis and interpretation were performed using established protocols described in earlier publications (Correa-Ascencio & Evershed, 2014). All solvents used were HPLC grade (Rathburn), and the reagents were analytical grade (typically > 98% of purity). Briefly, ~ 2 g of potsherd was sampled, and surfaces were cleaned with a modeling drill to remove exogenous lipids. The cleaned sherd powder was crushed in a solvent-washed mortar and pestle and weighed into a furnaced culture tube (I). An internal standard was added (20 µg *n*-tetratriacontane; Sigma-Aldrich Company Ltd.) together with 5 mL of H_2SO_4/MeOH 2–4% ($\delta^{13}C$ value measured), and the culture tubes were placed on a heating block for 1 h at 70 °C, mixing every 10 min. Once cooled, the methanolic acid was transferred to test tubes and centrifuged at 2500 rpm for 10 min. The supernatant was then decanted into another furnaced culture tube (II), and 2 mL of DCM-extracted double distilled water was added. In order to recover any lipids not fully solubilized by the methanol solution, 2 × 3 mL of *n*-hexane was added to the extracted potsherds contained in the original culture tubes, mixed well, and transferred to culture tube II. The extractions were transferred to clean, furnaced 3.5 mL vials, and blown down to dryness. Following this, 2 × 2 mL *n*-hexane was added directly to the H_2SO_4/MeOH solution in culture tube II and whirl mixed to extract the remaining residues and then transferred to the 3.5 mL vials and blown down until a full vial of *n*-hexane remained. Aliquots of the TLE's were derivatised using N,O-bis(trimethylsilyl)trifluoroacetamide (BSTFA) containing 1% trimethylchlorosilane (TMCS; Sigma-Aldrich Company Ltd.; 40 µL; 70 °C, 1 h), excess BSTFA was removed under nitrogen, and the derivatized FAMes were dissolved in *n*-hexane prior to GC, GC–MS, and GC-C-IRMS.

Firstly, the samples underwent gas chromatography using a GC fitted with a high-temperature non-polar column (DB1-HT; 100% dimethylpolysiloxane, 15 m × 0·32 mm i.d., 0.1-µm film thickness). The carrier gas was helium, and the temperature program comprised a 50 °C iso-thermal hold followed by an increase to 350 °C at a rate of 10 °C min^{-1} followed by a 10 min isothermal hold. A procedural blank (no sample) was prepared and analyzed alongside every batch of samples. Further compound identification was accomplished using GC–MS. FAMEs were introduced by autosampler onto a GC–MS fitted with a non-polar column, 50 m × 0.32 mm fused silica capillary column coated with an Rtx-1 stationary phase (100% dimethylpolysiloxane, Restek, 0.17 µm). The instrument was a ThermoScientific Trace 1300 gas chromatograph coupled to an ISQ single quadrupole mass spectrometer. Samples were run in full scan mode (*m/z* 50–650), and the temperature

program comprised an isothermal hold at 50 °C for 1 min, followed by a gradient increase to 300 °C at 10 °C min^{-1}, followed by an isothermal hold at 300 °C (15 min). The MS was operated in electron ionization (EI) mode at 70 eV. Data acquisition and processing were carried out using the HP Chemstation software (Rev. C.01.07 (27), Agilent Technologies), and Xcalibur software (version 3.0). Peaks were identified based on their mass spectra and GC retention times compared with the NIST mass spectral library (version 2.0).

Carbon isotope analyses by GC-C-IRMS were carried out using a GC Agilent Technologies 7890A coupled to an Isoprime 100 (EI, 70 eV, three Faraday cup collectors *m/z* 44, 45, and 46) via an IsoprimeGC5 combustion interface with a CuO and silver wool reactor maintained at 850 °C. Instrument accuracy was determined using an external FAME standard mixture (C_{11}, C_{13}, C_{16}, $C_{21,}$ and C_{23}) of known isotopic composition. Samples were run in duplicate, and the average was recorded. The $\delta^{13}C$ values are the ratios $^{13}C/^{12}C$, expressed relative to the Vienna Pee Dee Belemnite, calibrated against a CO_2 reference gas of known isotopic composition. The instrument error was ± 0.3‰. Data processing was carried out using Ion Vantage software (version 1.6.1.0, IsoPrime).

Results

Pottery Compositional Classification

In the thin sections, all but two of the 62 sherds have a related petrographic composition characterized by angular inclusions of plutonic igneous origin in a non-calcareous clay matrix. They can be subdivided in terms of the abundance of the mineral intergrowth perthite, which is common in two-thirds of the analyzed ceramics (perthite-rich granitic fabric) but not in the others (granitic fabric). The granitic fabric sherds contain poorly sorted angular inclusions of microcline, plagioclase, and weathered iron-containing alkali feldspar together with quartz and ferruginous grains (Fig. 3A, B). Argillaceous inclusions, iron-rich rock fragments with quartz inclusions, and small grains of zircon, biotite, and amphibole are also present in low abundance. The clay source used to produce the ceramics of this fabric is likely to have derived from the weathering of coarse-grained granitic igneous rock, such as granodiorite or quartz diorite, which could have been used without significant modification. The perthite-rich granitic fabric contains similar poorly sorted angular inclusions derived from granitic igneous rock. However, it differs in terms of the presence of significant quantities of perthitic feldspar (Fig. 3B, C) and a lower proportion of microcline. This suggests the use of coarse untempered clay derived from the weathering of a related but compositionally distinct, acid-intermediate plutonic rock. Samples JM011 and JM022 of the grog fabric are characterized by poorly sorted inclusions of grog, quartz, and feldspar (Fig. 3D, E), as well as rare amphibole, biotite, and chert. While the presence of quartz, feldspars, biotite, and amphibole suggest that granitic rock was the source of the mineral inclusions, their more rounded nature and lower concentration indicates that these originated from a sedimentary clay source. Grog inclusions testify to the addition of temper of crushed sherds of a similar ceramic composition.

The accuracy of the "UCL pXRF < 10% Ca calibration 2" over the standards that fall within the range of composition found in earthenware archaeological ceramics revealed that 11 of the 15 measured elements (Ca, Fe, Ga, K, Mn, Nb, Rb, Sr, Ti, Zn, Zr) had an average error of ≦25% relative difference between the certified and measured values (OSM 1). The Prolene film covering the powdered CRM samples will have absorbed X-rays and could have affected the counts of some or all of the elements, meaning that the performance may be slightly better than determined here. The element Ca was removed from the dataset because several samples had visible calcite encrustation, which was registered in the pXRF data, even after abrading the analyzed surface. The remaining ten elements (Table 2) were subjected to PCA before and after transformation to base 10 logarithms and the geometric mean. The latter two transformations did not improve the PCA in terms of the discrimination of chemical groups, so the raw non-transformed data was used (Table 2).

A plot of the first two principal components, which explain 66% of the total variance in the multivariate dataset, reveals the presence of two clear chemical groups and a single outlier (Fig. 4A). Sherds of chemical group 1 are defined by their higher values for the elements K, Mn, Nb, and Rb, and of chemical group 2 by their lower values for these elements,

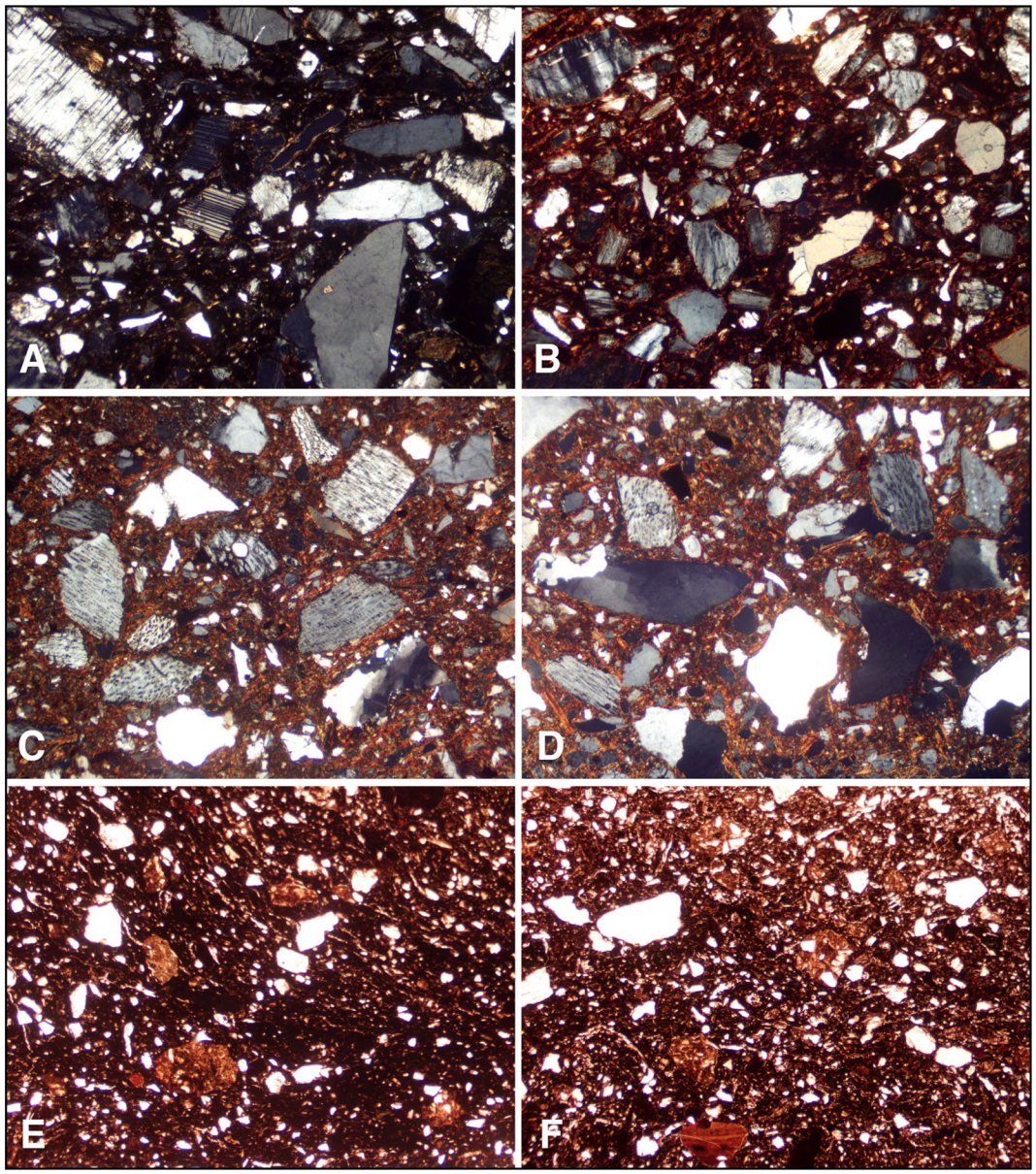

Fig. 3 Thin section photomicrographs of Jebel Moya pottery sherds belonging to the granitic fabric (**A** and **B**), the perthite-rich granitic fabric (**C** and **D**), and the grog fabric (**E** and **F**) detected in this study. Images were taken in crossed polars (XP). Image width = 2.9 mm

as well as its high Sr compared to chemical group 1 (Fig. 4B; Table 2). The two chemical groups correspond well to the granitic fabric (chemical group 1) and the perthite-rich granitic fabric (chemical group 2; Fig. 4C; Table 3). The higher abundance of K and Rb in the chemical group 1/granitic fabric sherds may be explained by their proportion of microcline in thin sections. The chemical group 2/perthite-rich granitic fabric samples have a higher K/Rb ratio supporting the idea that they were made from clay derived from a distinct, though related, igneous source and/or the clay was less weathered. One of the grog fabric sherds plots in chemical group 1 in the PCA, while the other occurs as an outlier due to its higher values

Table 2 Geochemical composition and classification of the 62 pottery sherds as determined by pXRF, including data on elements with ≦25% relative difference used in multivariate statistical classification and corresponding thin section petrographic classification

			Element (ppm)										
Sample number	Fabric	Chemical group	Fe	Ga	K	Mn	Nb	Rb	Sr	Ti	Zn	Zr	K/Rb ratio
JMC010	Granitic fabric	1.1	58,670	23	20,500	10,758	23	95	396	4580	111	459	216
JMC012	Granitic fabric	1.1	49,843	21	20,400	2038	22	101	351	5065	119	504	202
JMC015	Granitic fabric	1.1	48,766	24	32,150	556	23	108	486	4596	96	402	298
JMC026	Granitic fabric	1.1	46,394	22	37,950	360	20	94	341	4471	71	415	404
JMC029	Granitic fabric	1.1	48,022	21	25,500	310	18	89	361	4816	79	343	287
JMC030	Granitic fabric	1.1	42,479	22	34,500	867	23	106	308	4941	107	514	325
JMC040	Granitic fabric	1.1	54,276	23	30,800	669	30	88	283	6104	164	528	350
JMC060	Granitic fabric	1.1	44,775	24	34,950	617	21	106	329	4866	77	402	330
JMC062	Granitic fabric	1.1	47,133	22	29,750	561	21	104	400	4902	94	464	286
JMC011	Grog fabric	1.1	49,124	23	27,900	1526	24	94	470	5423	173	367	297
Average chem group 1.1			48,948	23	29,440	1826	23	99	373	4976	109	440	299
JMC002	Granitic fabric	1.2	41,331	22	49,350	496	20	150	284	5084	69	380	329
JMC003	Granitic fabric	1.2	43,080	20	40,367	352	18	137	281	5011	50	274	295
JMC006	Granitic fabric	1.2	35,176	22	52,550	254	18	160	442	4931	45	310	328
JMC016	Granitic fabric	1.2	40,940	21	41,550	403	19	141	407	5094	104	402	295
JMC023	Granitic fabric	1.2	35,244	22	37,850	269	16	170	277	4310	63	294	223
JMC024	Granitic fabric	1.2	30,737	22	47,400	294	16	165	285	4122	54	269	287
JMC025	Granitic fabric	1.2	31,420	22	38,750	302	17	150	275	3720	70	305	258
JMC032	Granitic fabric	1.2	35,155	22	34,300	486	19	155	299	4439	67	374	221
JMC061	Granitic fabric	1.2	30,795	20	59,100	210	17	126	392	4469	40	373	469
Average chem group 1.2			35,986	21	44,580	341	18	150	327	4576	62	331	301
Average chem group 1			42,808	22	36,611	1123	20	123	351	4787	87	388	300
JMC001	Perthite-rich granitic fabric	2	32,849	21	30,600	285	9	54	755	4481	66	263	567
JMC004	Perthite-rich granitic fabric	2	34,680	20	23,600	452	11	53	516	6390	77	349	445
JMC005	Perthite-rich granitic fabric	2	26,998	17	33,400	683	6	54	691	3563	68	205	619
JMC007	Perthite-rich granitic fabric	2	35,481	21	23,850	418	9	43	612	4910	81	288	555
JMC008	Perthite-rich granitic fabric	2	38,665	20	25,800	213	9	44	631	3857	59	216	586
JMC009	Perthite-rich granitic fabric	2	33,577	23	18,433	2023	7	62	736	3577	102	222	297
JMC013	Perthite-rich granitic fabric	2	27,895	21	33,250	375	5	61	1081	3487	93	198	545
JMC014	Perthite-rich granitic fabric	2	32,685	22	27,700	680	10	72	620	3897	117	216	385
JMC017	Perthite-rich granitic fabric	2	46,595	23	22,300	753	10	40	636	4561	144	200	558
JMC018	Perthite-rich granitic fabric	2	28,826	18	38,050	192	5	66	660	3189	70	171	577

Table 2 (continued)

			Element (ppm)										
JMC019	Perthite-rich granitic fabric	2	29,035	21	29,400	388	9	68	777	4641	92	214	432
JMC020	Perthite-rich granitic fabric	2	29,177	17	21,600	774	8	47	738	4492	139	217	460
JMC021	Perthite-rich granitic fabric	2	38,515	20	28,950	705	11	57	696	5710	136	221	508
JMC027	Perthite-rich granitic fabric	2	35,558	24	23,700	473	7	58	795	3357	91	231	409
JMC028	Perthite-rich granitic fabric	2	34,602	22	21,650	165	9	59	706	4027	86	182	367
JMC031	Perthite-rich granitic fabric	2	32,261	20	21,000	229	6	47	660	3468	75	203	447
JMC033	Perthite-rich granitic fabric	2	36,742	21	30,450	202	8	49	595	4951	66	275	621
JMC034	Perthite-rich granitic fabric	2	28,149	22	46,700	305	8	62	540	3267	73	191	753
JMC035	Perthite-rich granitic fabric	2	31,168	24	32,000	383	7	52	713	4441	87	212	615
JMC036	Perthite-rich granitic fabric	2	29,676	21	40,300	298	7	69	684	3197	74	209	584
JMC037	Perthite-rich granitic fabric	2	22,888	20	33,600	222	5	57	533	3227	51	159	589
JMC038	Perthite-rich granitic fabric	2	32,522	20	33,100	291	8	56	588	4991	70	244	591
JMC039	Perthite-rich granitic fabric	2	30,659	21	32,000	288	7	54	598	4158	84	225	593
JMC041	Perthite-rich granitic fabric	2	29,731	22	25,000	373	9	56	600	4613	64	238	446
JMC042	Perthite-rich granitic fabric	2	31,821	20	33,150	227	7	60	586	3622	86	166	553
JMC043	Perthite-rich granitic fabric	2	48,176	20	30,740	467	13	48	571	6174	105	317	640
JMC044	Perthite-rich granitic fabric	2	22,813	17	33,500	418	7	65	577	2805	84	148	515
JMC045	Perthite-rich granitic fabric	2	38,798	21	27,375	391	8	59	555	5169	93	213	464
JMC046	Perthite-rich granitic fabric	2	33,009	21	38,300	506	11	67	552	4693	112	276	572
JMC047	Perthite-rich granitic fabric	2	36,075	21	21,550	263	9	59	896	5324	72	191	365
JMC048	Perthite-rich granitic fabric	2	37,327	22	19,250	303	10	49	629	4288	84	227	393
JMC049	Perthite-rich granitic fabric	2	31,603	18	22,250	217	6	50	593	3639	57	175	445
JMC050	Perthite-rich granitic fabric	2	34,478	22	38,450	420	11	65	537	3723	75	249	592
JMC051	Perthite-rich granitic fabric	2	31,130	19	20,350	356	8	48	706	4724	95	229	424
JMC052	Perthite-rich granitic fabric	2	33,492	22	16,967	254	9	62	539	3666	79	243	274
JMC053	Perthite-rich granitic fabric	2	24,544	22	24,800	189	6	49	707	3653	63	184	506
JMC054	Perthite-rich granitic fabric	2	28,833	19	22,050	254	7	39	555	4204	61	220	565
JMC055	Perthite-rich granitic fabric	2	37,516	21	38,300	358	8	50	452	4208	140	210	766
JMC056	Perthite-rich granitic fabric	2	25,629	20	26,567	365	6	61	773	2805	65	151	436
JMC057	Perthite-rich granitic fabric	2	33,061	23	20,150	295	6	55	784	3675	86	205	366
JMC058	Perthite-rich granitic fabric	2	38,395	21	20,850	117	9	47	723	4757	55	195	444
JMC059	Perthite-rich granitic fabric	2	31,675	17	19,133	474	9	45	594	4477	66	211	425
Average chem group 2			32,793	21	27,861	406	8	55	655	4192	84	218	**507**
JMC022	Grog fabric	Outlier	63,183	17	18,500	1542	28	53	409	9878	109	313	349

for the elements Fe and Ti (Fig. 4C; Table 2). This suggests that the two samples may not share the same base clay despite containing grog. Plotting the elements Rb and Fe against each other makes it possible to discern a compositional split within chemical group 1, which is not readily apparent in the granitic fabric in thin-section despite the sherds containing some heterogeneity (Fig. 4D; Table 2). This is likely to indicate the use of a slightly different clay source, as no difference between these sherds was visible in the thin section.

Organic Residue Analysis

Analysis of the total lipid extracts (TLEs, $n=50$), using GC and GC–MS, revealed that nine of the 50 sherds (18%) contained sufficient concentrations (>5 μg g^{-1}) which can be reliably interpreted (Evershed, 2008; Table 3). Lipid concentrations were generally low. The extracts comprised two main lipid profiles. The first was dominated by free fatty acids, palmitic ($C_{16:0}$) and stearic ($C_{18:0}$), typical of a degraded animal fat ($n=6$, Fig. 5a) (e.g., Berstan et al., 2008; R. P. Evershed et al., 1997) with the second ($n=3$) also containing a sequence of abundant long-chain fatty acids, in distributions generally indicative of plant processing.

GC-C-IRMS analyses were carried out on six samples typical of degraded animal fats (Table 3, Fig. 6) to determine the $\delta^{13}C$ values of the major fatty acids, $C_{16:0}$ and $C_{18:0}$, and ascertain the source of the extracted lipids. The $\delta^{13}C$ values of the $C_{16:0}$ and $C_{18:0}$ fatty acids reflect their biosynthetic and dietary origin, allowing non-ruminant and ruminant adipose and ruminant dairy fats to be distinguished (Copley et al., 2003; Craig et al., 2012; Dunne et al., 2012). Ruminant dairy fats are differentiated from ruminant adipose fats when they display $\Delta^{13}C$ values of less than -3.1 ‰ (Dunne et al., 2012; Salque, 2012).

Lipid residue results for sherds, displaying typical degraded animal products, show that two vessels, JMC2330 and JMC2359, plot in the ruminant dairy region with $\Delta^{13}C$ values of -5.0 and -3.2 ‰, respectively (Table 2). However, it should be noted that vessel JMO2359 plots at the extent of the range, suggesting some mixing of dairy and ruminant carcass products. Three vessels (JMC2331, JMC2335, and JMC2351) plot in the ruminant adipose region with $\Delta^{13}C$ values of -2.2, -0.9, and -0.9 ‰, respectively (Table 3). The remaining vessel (JMO2360) plots between the ruminant and non-ruminant/plant regions, with a $\Delta^{13}C$ value of -0.6 ‰, suggesting either the mixing of ruminant and non-ruminant animal fats (or, possibly, plants) contemporaneously or during the lifetime of use of the vessel (Mukherjee, 2004; Mukherjee et al., 2005).

Notably, the second lipid profile, seen in three sherds (JMC2317, JMC2342, and JMC2354), differed from a typical animal product, comprising low abundances of C_{16} and C_{18} fatty acids but sequences of even-numbered long-chain fatty acids (LCFAs) in much higher abundance, containing C_{20} to C_{30} carbon atoms, generally dominated by the C_{26} (Fig. 5B). These LCFAs are strongly indicative either of an origin in leaf or stem epicuticular waxes (Bianchi, 1995; Kunst & Samuels, 2003; Tulloch, 1976) or possibly suberin (Kolattukudy, 1981; Pollard et al., 2008; Walton, 1990), an aliphatic polyester found in all plants. Although primarily found on the surface of plant leaves, sheaths, stems, and fruits, epicuticular waxes are also associated with other plant organs, i.e., seed oils and coats, flowers, bark, and husks (Bianchi, 1995). Fatty acids can be found in high abundance in some plants; for example, waxes from the leaves of the sorghum plant comprise nearly 40% very long-chain fatty acids (Bianchi, 1995). However, these LCFAs are not diagnostic to families of plants and so cannot be used as anything other than a general indicator for plant processing.

Discussion

The geology of the Gezira Plain is dominated by unconsolidated Tertiary and Quaternary sedimentary rocks, Pre-Cambrian basement, including schists, and igneous intrusions (Fig. 1a). The latter, which form the rocky hills of Jebel Moya and neighboring Jebel Saqadi, are composed of granite, containing the quartz, perthite, orthoclase, albite-oligoclase, biotite, and minor amphibole. Other igneous rocks include sills and plugs of basalt that are exposed at Sennar and west of Omdurman (Vail, 1982, p. 54). Cretaceous Nubian sandstone, siltstone, and mudstone occur to the northeast and northwest, where the Blue and White Nile rivers converge.

The petrographic composition of the majority of the analyzed sherds suggests the use of clay derived

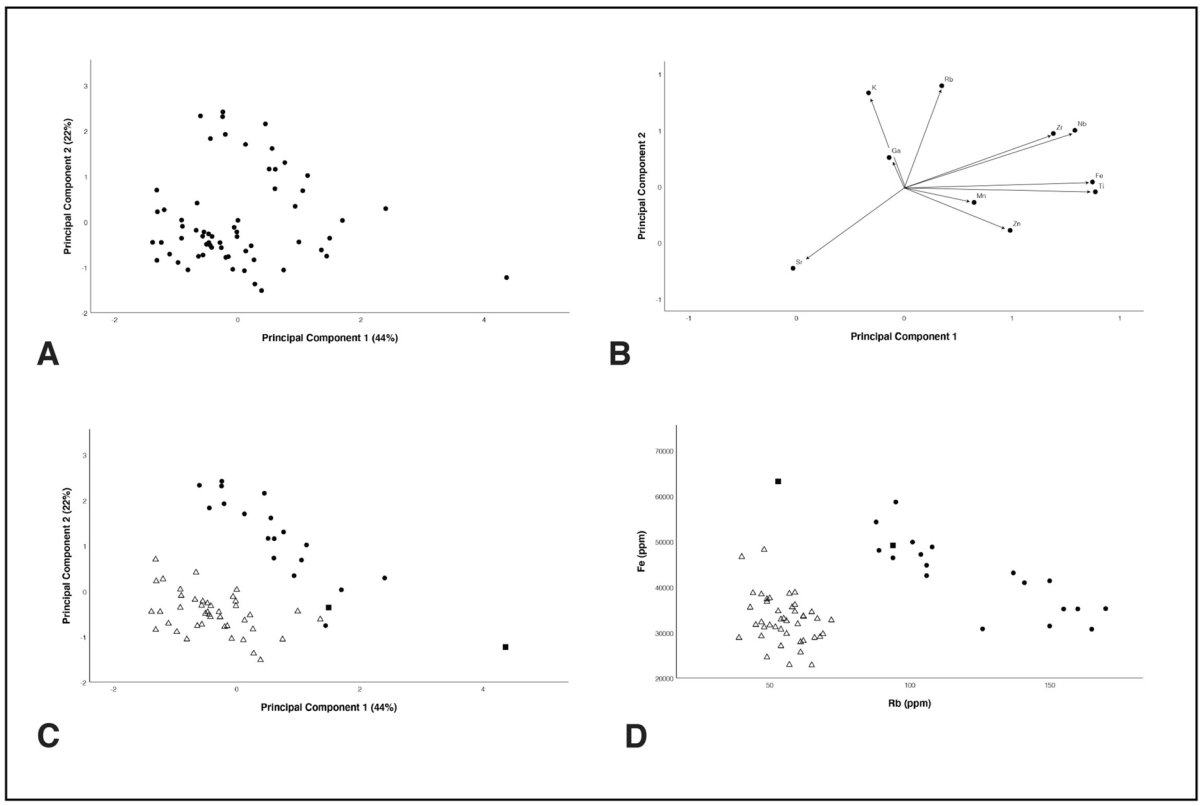

Fig. 4 Geochemical classification of the 62 pottery sherds. **A** Scatterplot of principal components analysis (PCA) scores using raw data from 10 elements (Fe, Ga, K, Mn, Nb, Rb, Sr, Ti, Zn, Zr) showing the existence of two chemical groups plus one outlier. **B** Loading plot, showing the influence of the 10 elements on the first two principal components. **C** PCA scatterplot with samples labeled by petrographic fabric. **D** Scatterplot of values for the elements Rb and Fe revealing compositional split in chemical group 1. Granitic fabric = closed circles; perthite-rich granitic fabric = open triangles, grog fabric = closed squares. For chemical group membership of individual samples and elemental characteristics of chemical groups and outliers, see Table 2

Table 3 Lab number, context, lipid concentration (μg g^{-1}), $\delta^{13}C$ and $\Delta^{13}C$ values, and attributions of pottery lipid residues from Jebel Moya

Laboratory number	Context	Lipid concentration (ug g^{-1})	$\delta^{13}C_{16:0}$	$\delta^{13}C_{18:0}$	$\Delta^{13}C$	Attribution
JM02317	Trench 1, Spit 3	312.6	-	-	-	Plant
JM02330	Trench 1, Spit 4	19.9	−19.2	−24.2	−5	Ruminant dairy
JM02331	Trench 1, Spit 5	119.5	−22	−24.2	−2.2	Ruminant adipose
JM02335	Trench 2, Spit 8	28.9	−23.8	−24.7	−0.9	Ruminant adipose
JM02342	Trench 2, Spit 8	109.3	-	-	-	Plant
JM02351	Trench 2, Spit 8	20.8	−16	−16.9	−0.9	Ruminant adipose
JM02354	Trench 4, Spit 4	90.7	-	-	-	Plant
JM02359	Trench 4, Spit 7	53.5	−21.1	−24.3	−3.2	Ruminant dairy
JM02360	Trench 4, Spit 7	617.3	−22.7	−23.3	−0.6	Ruminant/non-ruminant/plant

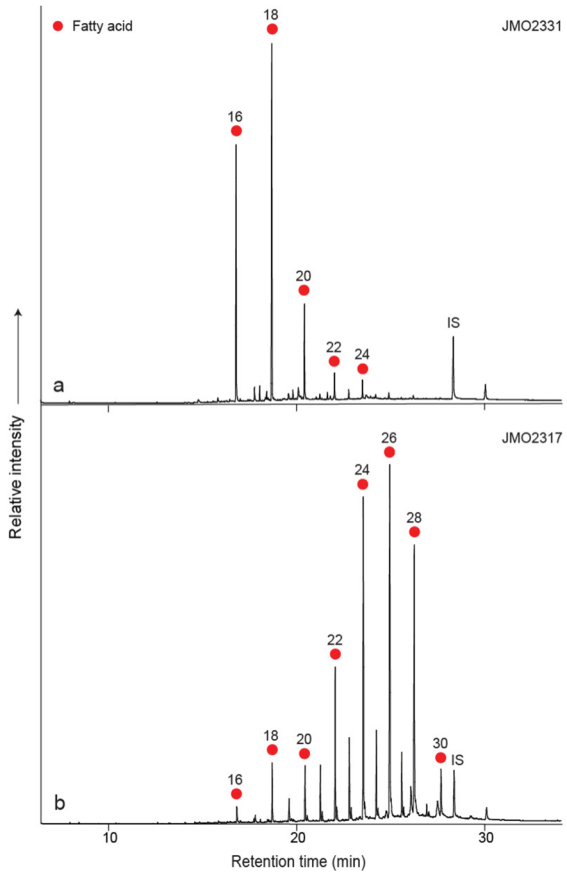

Fig. 5 Partial gas chromatograms of acid-extracted FAMEs from pottery extracts. **a** Sample JMO2331; **b** Sample JMO2317. Circles, *n*-alkanoic acids (fatty acids, FA); IS, internal standard, C_{34} *n*-tetratriacontane. Numbers denote carbon chain length

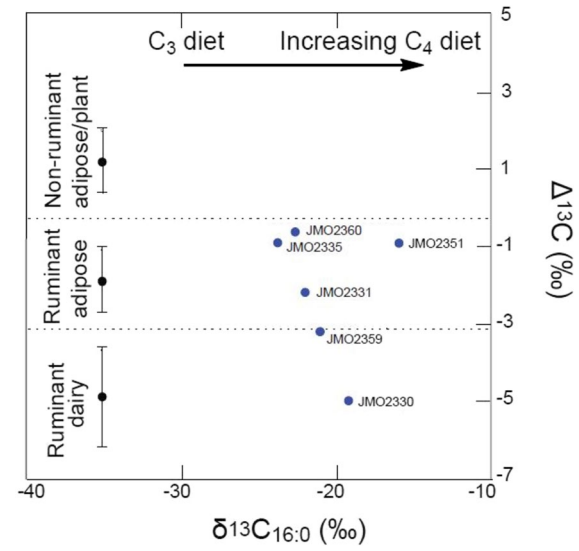

Fig. 6 Graph showing the $\Delta^{13}C$ ($\delta^{13}C_{18:0} - \delta^{13}C_{16:0}$) values. The ranges represent the mean ± 1 s.d. of the $\Delta.^{13}C$ values for a global database comprising modern reference animal fats from Africa (Dunne et al., 2012), UK (animals raised on a pure C_3 diet; Dudd & Evershed, 1998), Kazakhstan (Outram et al., 2009), Switzerland (Spangenberg et al., 2006), and the Near East (Gregg et al., 2009)

from acidic plutonic igneous rock such as granite. The mineral assemblage detected correlates well with the general description above of the granite bodies that form the Jebel Moya and Jebel Sagadi massifs, particularly the presence of perthite, which is characteristic of the perthite-rich granitic fabric/chemical group 2 (Fig. 3). With this in mind, it seems plausible that the raw materials for these perthite-rich granitic fabric/chemical group 2 sherds were sourced locally from coarse clay formed by the weathering of the granite, as suggested by the previous analysis of three sherds from the site in the study of Brass (2015). The sand samples collected from Jebel Moya confirm the presence of degraded igneous material of the composition reported for the area and that seen in thin-section in the pottery, including perthite.

The significance of the two distinct but related granite-derived fabrics, as well as the two chemical subgroups of the granitic fabric/chemical group 1, is not clear given the lack of further information on the geology of Jebel Moya and other igneous outcrops in the Gezira Plain and the absence of field samples from other locations. However, they seem likely to represent several separate clay sources. Large granite bodies typically contain mineralogical and chemical variations resulting from several intrusion events and/or the fractionation of magma during its slow cooling underground. With this in mind, it is possible to imagine potters sourcing compositionally similar clay from several places around Jebel Moya and the surroundings, including Jebel Saqadi, albeit containing mineralogical and chemical differences that were not perceptible to the eye or the touch. Equally, one or more of the three granitic compositions could represent pottery made at another location, for example, the site of Jebel Saqadi (Fig. 1a). Whether the granite bedrock of this massif is distinct from that of Jebel Moya is not clear.

Archaeological evidence exists for the occupational activity at Jebel Saqadi (Crawford & Addison,

1951), including mudbrick architecture and pottery sherds. The latter is claimed to bear similarities with the pottery of Assemblage 3 of Jebel Moya, as well as the agro-pastoral village Abu Geili, along the Blue Nile (Fig. 1a). The presence of two main granitic compositions within the ceramics analyzed from Jebel Moya may therefore indicate the existence of local ceramics, as well as non-local material produced at Jebel Saqadi.

The site of Abu Geili is located c. 30 km east of Jebel Moya along the banks of the Blue Nile (Fig. 1a). Also, it contains pottery with stylistic links to that of Jebel Moya (Fig. 2D). The latter includes grooved sherds that belong to the granitic fabric/chemical group 1 that could not have been produced at Abu Geili due to its different underlying geology and may therefore be tentatively taken to suggest the transport of ceramics from Jebel Moya. Abu Geili is situated in an area of Cenozoic sedimentary rock, overlain by recent alluvium. While data on the exact composition of these strata were not available and pottery from the site has not yet been studied compositionally, it may be that the two petrographically and chemically distinct sherds of the grog fabric analyzed in this study could have been made here and thus represent the transport of material in the other direction to Jebel Moya. However, the chemical correspondence of one of these samples with chemical group 1.1 might not support this suggestion. An alternative source area is the Northern Gezira, where Cretaceous sedimentary rocks, including mudstone outcrop, occur (Fig. 1a). The potential small-scale movement of pottery detected here could have occurred as a result of savanna herding, for which ceramics may have been essential tools for processing milk, meat, and/or blood (e.g., Grillo, 2012, p. 195–203), with such movements tied into relationships with neighboring communities.

The stylistic variability of the analyzed ceramics does not correlate with their compositional characteristics, as defined in this study. Multiple decorative motifs made using different tools are on the sherds belonging to all petrographic and chemical groups. Equally, no clear pattern exists in terms of the distribution of the various petrographic and chemical groups across the different spits in Assemblage 3 of Jebel Moya based on the samples analyzed in this study. Sherds of the granitic fabric/chemical group 1 and its subgroups and the perthite-rich granitic fabric/chemical group 2 are present in the lower, middle, and upper spits. Only three Assemblage 1 and 2 sherds were included for comparative purposes, all made of the granitic fabric/chemical subgroups 1.1 and 1.2. The absence of material belonging to the perthite-rich granitic fabric/chemical group 2 and the grog fabric among these samples cannot be considered significant.

The low lipid recovery rate from the ceramics (Table 2), which underwent organic residue analysis, could suggest that the vessels were not subjected to sustained use. Alternatively, it may be a feature of the preservation conditions at the site. Nonetheless, the results demonstrate that two vessels were routinely used to process ruminant dairy products, and another three vessels were used to process ruminant carcass products. A sixth vessel was likely used to process a mixture of ruminant and non-ruminant carcass products. The non-ruminant signal could originate from wild pigs or boar, if present in the area, other non-ruminant wild fauna, or possibly, plants.

The $\delta^{13}C_{16:0}$ values of the fatty acids extracted from the potsherds provide valuable information on environmental conditions and possible animal management strategies. Here, the $\delta^{13}C_{16:0}$ values from the animal products range from -23.8 to -16.0 ‰, possibly suggesting the processing of products from animals subsisting on varied C_3/C_4 diets or that animals may have been managed differently, i.e., through seasonal movements. The somewhat enriched values suggest locally available C_4 plants, confirmed by domesticated sorghum at the site. Certainly, cattle eat wild sorghum and other C_4 grasses (Snow, 1948).

As a substantial faunal assemblage is developed from ongoing excavations (see Brass et al., 2019, for a preliminary analysis from the first 2017 season), then it would be useful to compare the lipid results to the faunal assemblage to determine what animals may have been processed in the vessels and gain further insight into possible animal husbandry strategies. The bones of cattle (*Bos* sp.), goats (*Capra hircus*), and probably sheep (*Ovis aries*) are found in the sampled stratigraphic sequences, confirming, together with the chemical evidence, that the exploitation of domesticates for their meat and milk products was a key feature of subsistence strategies at the site. It should, however, be noted that it is difficult to make broad generalizations on animal management based on small sample sizes. Also noteworthy is the likely

importance of dedicated plant processing at the site, a tradition with a long history to the north, i.e., at Khor Shambat (Dunne et al., 2021), Sphinx (Garcea et al., 2020), and al-Khiday in Central Sudan (Dunne et al., 2022).

Conclusion

Our research set out to answer three questions: the origin of clay sources, the identification of pottery traditions and their longevity, and the function of vessels during the period encompassed by Assemblage 3 at Jebel Moya. Our method of spit excavation has resulted in a finely detailed breakdown of changing pottery attributes and decoration motifs (Brass & Vella Gregory, 2021). This study shows that during the first millennium BC, pottery was overwhelmingly made using locally available clay. Over the course of a millennium, people do not appear to have changed their clay sources or recipes, based on the analyzed samples. No correlation exists between the motifs and tools used to decorate the locally manufactured ceramics and their petrographic and chemical composition. This suggests a strong manufacturing tradition.

Some sherds were made from a source with related but distinctive geological characteristics, such as Jebel Saqadi, 20 km to the north (Brass, 2015). Rare sherds of a very different paste composition, made from raw materials that may not have been available at Jebel Moya or Jebel Saqadi, suggest the existence of pottery from a third location. One potential candidate is the contemporaneous site of Abu Geili, c. 30 km to the east, implying the transport of pottery and communication between the people of Jebel Moya and those inhabiting the banks of the Blue Nile. Jebel Moya Assemblage 3 sherds have been identified at Abu Geili (Brass, 2016; Crawford & Addison, 1951). This and the connection with Jebel Saqadi should be tested by future compositional analysis of pottery and raw material samples from these sites and elsewhere in southern Gezira.

Seen only through a compositional lens, traditions appear to be fairly static. People did not change their clay sources or recipes; instead, they focused on the sheer diversity of visual elements of pottery: while motifs do persist, they also eventually change (see Brass & Vella Gregory, 2021 for the detailed study of how visual decoration of pottery reveals aspects of identity and communities of practice).

Finally, with regard to vessel function, while it should be noted that this is a small dataset, some preliminary observations on subsistence practices at Jebel Moya can be made. Our results demonstrated that at least some pottery was used to process animal products, including ruminant dairy and carcass products and non-ruminant carcass products. This is verified by the zooarchaeological data, which confirms the presence of domesticated cattle, sheep, and goats at the site. The importance of vessels dedicated to plant processing is noteworthy, suggesting the importance of a broad range of resources to people at Jebel Moya.

Together, these results illustrate the importance of integrating various strands of archaeological data. The petrographic results are also the first of its kind for the first millennium BC, south of Khartoum. While pottery production from Al Khiday, immediately south of Omdurman along the White Nile, has been analyzed, it focused on Mesolithic and Neolithic pottery (Del Sasso et al., 2014). In particular, this study provides a way to address complex questions relating to mobility and change. Thus, while the composition of clay did not change much across a millennium, our sequence enabled us to trace other changes. Equally, the zooarchaeological data must be read with residue studies. This was a time of fairly rapid climatic change, and a better understanding of how the people were moving in the landscape, what foods they were consuming, how they were consuming, and how they were constructing social identities and traditions through their pottery in a region where today there are a number of different social cultures interacting are vital questions only partially answered by this study. This integrated approach to material culture will enable us to expand the research to materials and remains from subsequent field seasons. It will also assist in answering questions on mobility in the southern Gezira in finer detail.

Appendix 1

Table 4 Comparison of certified and measured values for 14 reference materials used to assess the performance of UCL pXRF calibration 2 for < 10% Ca ceramics over the range of concentrations found in earthenware archaeological ceramics

		Ca		Co		Cu		Fe		Ga	
Ceramics min		0.2		0.0003		0.0000		0.81		no data	
Ceramics max		20.94		0.0087		0.0334		9.92		no data	
Standard	**Details**	**Certified**	**Accuracy**	**Certified**	**Accuracy**	**Certified**	**Accuracy**	**Certified**	**Accuracy**	**Certified**	**Accuracy**
CGL 111	Rare earth ore	18.23	6.75	0.0032	43.08	0.0147	26.56	9.51	42.10		
CGL 002	Alkaline granite	0.277	3.79			0.0007	1041.57			0.0057	19.58
CGL 006	Nepheline syenite	1.63	15.80			0.0026	63.58	1.839	12.93	0.0023	18.79
CGL 007	Basalt	3.87	19.56	0.0036	14.38	0.0032	119.67	6.888	12.93	0.0023	20.69
GBM30612	Certified Ore Grade Base Metal			0.00225	72.03			3.595	22.25		
SARM 1	NIM-G Granite	0.56	10.66			0.0012	374.47	1.40	0.62	0.0027	2.05
SARM 41	Carbonaceous Shale	1.07	15.11	0.0015	1.60			2.96	14.08	0.0020	3.76
SARM 42	Soil	0.64	14.48	0.0035	48.99	0.0017	288.75	3.27	4.65	0.0012	17.44
SARM 44	Sillimanite Schist	0.10	28.90	0.0008	34.47	0.0010	372.03	1.44	4.97	0.0055	13.06
SARM 45	Kinzingite	0.56	15.53	0.0041	5.88	0.0011	196.35	8.81	5.78	0.0035	5.72
SARM 48	Fluorspar Granite	6.36	16.23			0.0010	330.69				
SARM 50	Dolerite	7.72	13.89	0.0040	20.57			7.96	18.14		
SARM 52	Stream Sediment	0.26	9.14	0.0081	13.46	0.0219	34.75			0.0015	100.00
SARM 69	Ceramic-1	1.69	20.98	0.0028	0.81	0.0046	143.25	5.02	0.17		
Average accuracy			**14.68**		**25.53**		**271.97**		**12.60**		**22.34**

Table 4 (continued)

		K		Mn		Nb		Pb		Rb	
Ceramics min		0.39		0.01		no data		0.0000		0.0001	
Ceramics max		4.59		0.24		no data		0.0099		0.0230	
Standard	**Details**	**Certified**	**Accuracy**	**Certified**	**Accuracy**	**Certified**	**Accuracy**	**Certified**	**Accuracy**	**Certified**	**Accuracy**
CGL 111	Rare earth ore	0.76	35.91	0.1080	34.20					0.0043	18.75
CGL 002	Alkaline granite	2.97	8.68			0.0064	0.16	0.0063	64.38		
CGL 006	Nepheline syenite					0.004	16.57			0.0207	19.02
CGL 007	Basalt	3.31	0.18	0.1007	12.22	0.0052	14.63	0.0009	70.22	0.0063	19.50
GBM30612	Certified Ore Grade Base Metal										
SARM 1	NIM-G Granite	4.14	7.86	0.0160	30.27						
SARM 41	Carbonaceous Shale	1.15	9.32	0.0460	6.95	0.0008	4.78	0.0030	53.56	0.0059	0.40
SARM 42	Soil	0.37	30.26	0.0770	8.19	0.0008	60.50	0.0010	65.12	0.0022	1.60
SARM 44	Sillimanite Schist			0.0230	19.51	0.0096	10.82	0.0030	41.51	0.0013	27.93
SARM 45	Kinzingite	2.64	0.98	0.0770	13.00	0.0027	8.39	0.0020	2.76	0.0142	7.45
SARM 48	Fluorspar Granite	3.54	4.87	0.0150	40.01	0.0202	52.35				
SARM 50	Dolerite	0.51	5.98	0.1320	13.21	0.0010	48.21	0.0025	53.89	0.0014	30.06
SARM 52	Stream Sediment			0.2090	0.22	0.0011	26.22			0.0020	20.77
SARM 69	Ceramic-1	1.63	3.91	0.1000	2.43	0.0009	0.56	0.0014	49.74	0.0066	5.08
Average accuracy			**10.79**		**16.38**		**22.11**		**50.15**		**15.06**

Table 4 (continued)

		Sr		Ti		Y		Zn		Zr	
Ceramics min		0.0045		0.12		0.00		no data		0.00317	426.77
Ceramics max		0.0579		0.73		0.02		no data		0.0427	
Standard	**Details**	**Certified**	**Accuracy**	**Certified**	**Accuracy**	**Certified**	**Accuracy**	**Certified**	**Accuracy**	**Certified**	**Accuracy**
CGL 111	Rare earth ore							0.0600	39.85		
CGL 002	Alkaline granite					0.0023	100.00	0.0092	25.72	0.004	4.91
CGL 006	Nepheline syenite			0.222	22.22	0.0023	26.34	0.0098	6.02		
CGL 007	Basalt					0.002	24.11	0.0114	2.65	0.0287	8.92
GBM30612	Certified Ore Grade Base Metal							2.063	7.35		
SARM 1	NIM-G Granite							0.0050	11.78	0.0300	9.05
SARM 41	Carbonaceous Shale	0.0054	6.39	0.3300	5.05	0.0017	22.65	0.0076	30.42	0.0146	2.32
SARM 42	Soil			0.2160	12.86	0.0011	20.08	0.0044	12.62	0.0192	5.37
SARM 44	Sillimanite Schist					0.0084	6.48	0.0271	28.86	0.0406	10.54
SARM 45	Kinzingite	0.0092	8.94			0.0063	11.77	0.0074	13.15	0.0322	7.60
SARM 48	Fluorspar Granite							0.0053	10.47	0.0300	15.61
SARM 50	Dolerite	0.0195	15.53	0.5160	14.92	0.0023	22.96	0.0081	1.89	0.0086	17.53
SARM 52	Stream Sediment			0.7790	5.42	0.0020	29.47	0.0264	10.26	0.0250	4.75
SARM 69	Ceramic-1	0.0109	3.37	0.4660	0.83	0.0029	8.54	0.0068	3.20	0.0271	4.88
Average accuracy			**8.56**		**10.22**		**27.24**		**14.59**		**8.31**

Acknowledgements The excavation of Jebel Moya is funded by The British Institute for Libyan and Northern African Studies (formerly the Society for Libyan Studies). Brass, Vella Gregory, and Adam are grateful to the people of Jebel Moya for their generous enthusiasm, support, and hospitality and to our fantastic fieldwork team. We are also grateful to the National Corporation of Antiquities (NCAM) for their continued enormous and invaluable support.

Funding The authors thank the NERC for partial funding of the National Environmental Isotope Facility (NEIF; contract no. NE/V003917/1). We also thank NERC (contract no. NE/V003917/1), the European Research Council under the European Union's Seventh Framework Programme (FP/2007–2013), and European Research Council Grant Agreement number 340923 for funding GC–MS capabilities, and NERC (contract no. NE/V003917/1) and the University of Bristol for funding the GC-IRMS capabilities. Ian Bull, Alison Kuhl, and Helen Whelton are thanked for their technical help.

Accuracy is calculated using the formula (measured-certified)/certified)×100 and with relative error given in percentage. Ceramics compositional range is determined using data from Quinn et al. (2010), Day et al. (2011), Trave et al. (2014), and Quinn and Burton (2015).

References

Adamson, D. A., Clark, J. D., & Williams, M. A. J. (1987). Pottery tempered with sponge from the White Nile, Sudan. *African Archaeological Review, 5*, 115–127.

Addison, F. (1949). *Wellcome excavations in the Sudan: I, Jebel Moya, 1910–1914*. Oxford University Press.

Baxter, M. J. (2015). *Exploratory multivariate analysis in archaeology*. Percheron Press.

Berstan, R., Stott, A. W., Minnitt, S., Ramsey, C. B., Hedges, R. E. M., & Evershed, R. P. (2008). Direct dating of pottery from its organic residues: New precision using compound-specific carbon isotopes. *Antiquity, 82*(317), 702–713.

Bianchi, G. (1995). Plant waxes. In G. Hamilton (Ed.), *Waxes: Chemistry, molecular biology and functions.* The Oily Press Ltd.

Brass, M., & Vella Gregory, I. (2021). The chronological and social implications of the pottery from Jebel Moya. *Journal of Archaeological Science: Reports, 35*, 102677–102677.

Brass, M., Adam, A., & Wellings, J. (2018). New data from Jebel Moya and Shaqadud (central Sudan): Implications for Late Mesolithic interconnectivity with the Sahara. *Libyan Studies, 49*, 21–49.

Brass, M., Fuller, D. Q., MacDonald, K., Stevens, C., Adam, A., Kozieradzka-Ogunmakin, I., et al. (2019). New findings on the significance of Jebel Moya in the eastern Sahel. *Azania: Archaeological Research in Africa, 54*(4), 425–444.

Brass, M., Adam, A., Vella Gregory, I., Abdallah, R., Alawad, O., Abdalla, A., et al. (2020). The second season of excavations at Jebel Moya (south-central Sudan). *Libyan Studies, 51*, 126–140.

Brass, M. (2015). Interactions and pastoralism along the southern and southeastern frontiers of the Meroitic State, Sudan. *Journal of World Prehistory*, *28*(4).

Brass, M. (2016). *Reinterpreting chronology and society at the mortuary complex of Jebel Moya (Sudan).* Cambridge Monographs in African Archaeology 92, Archaeopress.

Burton, M., Quinn, P. S., Tamberino, A., & Levy, T. (2019). Ceramic composition at Chalcolithic Shiqmim, northern Negev desert, Israel: Investigating technology and provenance using thin section petrography, instrumental geochemistry, and calcareous nannofossils. *Levant, 50*, 237–257.

Burton, M., Quinn, P., Bennallack, K., Farahani, A., Howland, M. D., Najjar, M., et al. (2021). Ceramic technology at Wadi Fidan 61, an Early Pottery Neolithic site (ca. 6500 B.C.E.) in the Faynan region of Southern Jordan. *Journal of Archaeological Science Reports, 38*, 103029.

Copley, M. S., Berstan, R., Dudd, S. N., Docherty, G., Mukherjee, A. J., Straker, V., et al. (2003). Direct chemical evidence for widespread dairying in prehistoric Britain. *Proceedings of the National Academy of Sciences, 100*(4), 1524–1529.

Correa-Ascencio, M., & Evershed, R. P. (2014). High throughput screening of organic residues in archaeological potsherds using direct acidified methanol extraction. *Analytical Methods, 6*(5), 1330–1340.

Craig, O. E., Allen, R. B., Thompson, A., Stevens, R. E., Steele, V. J., & Heron, C. (2012). Distinguishing wild ruminant lipids by gas chromatography/combustion/isotope ratio mass spectrometry. *Rapid Communications in Mass Spectrometry, 26*(19), 2359–2364.

Crawford, O., & Addison, F. (1951). *Abu Geili, Saqadi and Dar el Mek. The Wellcome excavations in the Sudan*. Oxford University Press.

Dal Sasso, G., et al. (2014). Discriminating pottery production by image analysis: A case study of Mesolithic and Neolithic pottery from Al Khiday (Khartoum, Sudan). *Journal of Archaeological Science, 46*, 125–143.

Day, P., Quinn, P., Kilikoglou, V., & Rutter, J. A. (2011). World of goods: Transport jars and commodity exchange at the Late Bronze Age Harbor of Kommos, Crete. *Hesperia, 80*, 511–558.

Dudd, S. N., & Evershed, R. P. (1998). Direct demonstration of milk as an element of archaeological economies. *Science, 282*(5393), 1478–1481.

Dunne, J., Evershed, R. P., Salque, M., Cramp, L., Bruni, S., Ryan, K., et al. (2012). First dairying in green Saharan Africa in the fifth millennium BC. *Nature, 486*(7403), 390–394.

Dunne, J., Jórdeczka, M., Chłodnicki, M., Hardy, K., Kubiak-Martens, L., Hoyo, M.-D., et al. (2021). Holocene resource exploitation along the Nile: Diet and subsistence strategies of Mesolithic and Neolithic societies at Khor Shambat 1, Sudan. *Antiquity, 95*, 1–20.

Dunne, J., Salvatori, S., Maritan, L., Manning, K., Linseele, V., Gillard, T., et al. (2022). Wild food: Plants, fish and small animals on the menu for Early Holocene populations at al-Khiday, central Sudan. *African Archaeological Review, 39*, 255–281.

Evershed, R. P. (2008). Experimental approaches to the interpretation of absorbed organic residues in archaeological ceramics. *World Archaeology, 40*(1), 26–47.

Evershed, R. P., Mottram, H. R., Dudd, S. N., Charters, S., Stott, A. W., Lawrence, G. J., et al. (1997). New criteria for the identification of animal fats preserved in archaeological pottery. *Naturwissenschaften, 84*(9), 402–406.

Garcea, E., D'Ercole, G., Sterba, J., Dunne, J., Manning, K., Gillard, T., et al. (2020). Technological variability in forager's pottery productions at the early-mid Holocene site of Sphinx, western part of Jebel Sabaloka, Sudan. *Quaternary International, 555*, 110–125.

Gosselain, O. (2000). Materializing identities: An African perspective. *Journal of Archaeological Method and Theory, 7*(3), 187–216.

Gosselain, O. (2010). Exploring the dynamics of African pottery cultures. In R. Barndon, A. Engevik, & I. Øye (Eds.), *The archaeology of regional technologies: Case studies from the Palaeolithic to the Age of the Vikings* (pp. 193–226). The Edwin Mellen Press.

Gosselain, O., & Livingstone Smith, A. (2013). A century of ceramic studies in Africa. In P. Mitchell & P. Lane (Eds.), *The Oxford Handbook of African Archaeology* (pp. 117–130). Oxford University Press.

Gregg, M. W., Banning, E. B., Gibbs, K., & Slater, G. F. (2009). Subsistence practices and pottery use in Neolithic Jordan: Molecular and isotopic evidence. *Journal of Archaeological Science, 36*(4), 937–946.

Grillo, K. M. (2012). *The materiality of mobile pastoralism: Ethnoarchaeological perspectives from Samburu, Kenya*. Ph.D. thesis, Washington University in St. Louis.

Humphries, D. (1992). *The preparation of thin sections of rocks, minerals, and ceramics*. Oxford University Press.

Kolattukudy, P. E. (1981). Structure, biosynthesis, and biodegradation of cutin and suberin. *Annual Review of Plant Physiology, 32*(1), 539–567.

Kunst, L., & Samuels, A. L. (2003). Biosynthesis and secretion of plant cuticular wax. *Progress in Lipid Research, 42*(1), 51–80.

Lewis, M., Quinn, P., & Carter, R. (2020). Uruk expansion or integrated development? A petrographic and geochemical perspective from Gurga Chiya, Iraqi Kurdistan. *Journal of Archaeological Science Reports, 33*, 102516.

Ministry of Energy & Mines, Geological & Mineral Resources (1981) *Geological map of Sudan*. Khartoum. https://esdac.jrc.ec.europa.eu/content/geological-map-sudan

Mukherjee, A. J., Copley, M., Berstan, R., Clark, K., & Evershed, R. (2005). Interpretation of δ13C values of fatty acids in relation to animal husbandry, food processing and consumption in prehistory. In J. Mulville & A. Outram (Eds.), *The zooarchaeology of milk and fats*. Oxbow Books.

Mukherjee, A. J. (2004). *The importance of pigs in the Later British Neolithic: Integrating stable isotope evidence from lipid residues in archaeological potsherds, animal bone, and modern animal tissues*. Ph.D. thesis, University of Bristol.

Outram, A. K., Stear, N. A., Bendrey, R., Olsen, S., Kasparov, A., Zaibert, V., et al. (2009). The earliest horse harnessing and milking. *Science, 323*(5919), 1332–1335.

Pollard, M., Beisson, F., Li, Y., & Ohlrogge, J. B. (2008). Building lipid barriers: Biosynthesis of cutin and suberin. *Trends in Plant Science, 13*(5), 236–246.

Quinn, P. (2022). *Thin section petrography, geochemistry and scanning electron microscopy of archaeological ceramics*. Archaeopress.

Quinn, P., & Burton, M. (2015). Ceramic distribution, migration and cultural interaction among late prehistoric (ca. 1300–200 B.P.) hunter-gatherers in the San Diego region, southern California. *Journal of Archaeological Science Reports, 5*, 285–295.

Quinn, P., Day, P., & Kilikoglou, V. (2010). Keeping an eye on your pots: The provenance of Neolithic ceramics from Cyclops Cave on the Island of Youra, Greece. *Journal of Archaeological Science, 37*, 1042–1052.

Quinn, P., Ying, Y., Xia, Y., Li, X., Ma, S., Zhang, S., et al. (2020). Geochemical evidence for the manufacture, logistics and supply-chain management of Emperor Qin Shihuang's Terracotta Army. *China. Archaeometry, 63*(1), 40–52.

Salque, M. (2012.). *Regional and chronological trends in milk use in prehistoric Europe traced through molecular and stable isotope signatures of fatty acyl lipids preserved in pottery vessels*. Ph.D. thesis, University of Bristol.

Snow, O. (1948). Animal foodstuffs. In. J. D. Tothill (Ed.). Agriculture in the Sudan. Being a handbook of agriculture as practiced in the Anglo-Egyptian Sudan (pp. 668–687). Oxford University Press.

Sorresso, D., & Quinn, P. (2020). Re-examining shell-tempered Chickasaw pottery in post-contact Mississippi, USA. *Journal of Archaeological Science Reports, 32*, 102415.

Spangenberg, J. E., Jacomet, S., & Schibler, J. (2006). Chemical analyses of organic residues in archaeological pottery from Arbon Bleiche 3, Switzerland – Evidence for dairying in the late Neolithic. *Journal of Archaeological Science, 33*(1), 1–13.

Speakman, R., & Shackley, M. (2013). Silo science and portable XRF in archaeology: A response to Frahm. *Journal of Archaeological Science, 40*, 1435–1443.

Travé Allepuz, E., Quinn, P., López Pérez, M., & Padilla Lapuente, J. (2014). One hundred sherds of grey: Compositional and technological characterization of Medieval Greyware pottery production at Cabrera d'Anoia, Catalonia, Spain. *Archaeological and Anthropological Sciences, 6*, 397–410.

Tulloch, A. (1976). Chemistry of waxes of higher plants. In P. Kolattukudy (Ed.), *Chemistry and biochemistry of natural waxes*. Elsevier.

Tykot, R. (2016). Using nondestructive portable X-ray fluorescence spectrometers on stone, ceramics, metals, and

other materials in museums: Advantages and limitations. *Applied Spectroscopy, 70*, 42–56.

Vail, J. (1982). Geology of the central Sudan. In M. Williams & D. Adamson (Eds.), *A land between two Niles: Quaternary geology and biology of the Central Sudan* (pp. 51–64). A. A. Balkema.

Vella Gregory, I. (2020). Ordering the land beyond the Sixth Cataract: Imperial policy, archaeology and the role of Henry Wellcome. *Libyan Studies, 51*, 43–60.

Vella Gregory, I., Brass, M., & Kozieradzka-Ogunmakin, I. (2022). New radiocarbon dates from Jebel Moya (Sudan): 2500 years of burial activity. *Antiquity, 96*(388), 1015–1020.

Walton, T. (1990). Waxes, cutin and suberin. In J. Harwood & J. Boyer (Eds.), *Methods in plant biochemistry.* Academic Press.

Wilke, D., Rauch, D., & Rauch, P. (2016). Is non-destructive provenancing of pottery possible with just a few discriminative trace elements? *STAR: Science & Technology of Archaeological Research, 2*, 141–158.